JOURNAL OF CATALYSIS 148, 501–513 (1994)

Ammoxidation of Propane over Antimony–Vanadium–Oxide Catalysts

Roland Nilsson,* Thomas Lindblad,† and Arne Andersson*

*Department of Chemical Engineering II (Chemical Technology); and †Department of Inorganic Chemistry 1, University of Lund, Chemical Center, P.O. Box 124, S-221 00 Lund, Sweden

Received September 20, 1993; revised February 2, 1994

Catalysts belonging to the Sb–V–O system were prepared with various Sb/V ratios and were used for propane ammoxidation to acrylonitrile. XRD patterns of freshly prepared samples show those with excess vanadia to consist of V_2O_5 and $SbVO_4$, while $SbVO_4$ and α-Sb_2O_4 are constituents in the samples with a Sb/V ratio above unity. High rate and selectivity for propylene formation at low conversion are characteristic for samples with excess vanadia and considering XRD, Raman, infrared, and XPS results, this is explained by formation of amorphous vanadia spread over the surface of $SbVO_4$. Catalysts with both α-Sb_2O_4 and $SbVO_4$ phases are the most selective for acrylonitrile formation, a function that is linked to their ability to selectively transform intermediate propylene. XPS data suggest this function to be associated with the formation of suprasurface antimony sites on $SbVO_4$ as a result of migration of antimony from α-Sb_2O_4 during the catalytic process. Raman and infrared spectral features revealed that compared with $SbVO_4$, the samples with both α-Sb_2O_4 and $SbVO_4$ are more efficiently reoxidised during propane ammoxidation. Rate dependences on the partial pressures of reactants over a sample with excess α-Sb_2O_4 show that the adsorption of propane is the rate limiting step for propylene formation, and that acrylonitrile and carbon oxides are predominantly formed from the intermediate propylene in routes comprising nonequilibrated steps. Addition of water vapour results in an increase of rate and selectivity for acrylonitrile formation. The kinetic dependences indicate that for acrylonitrile formation it is advantageous to have a feed rich in propane and to use recirculation for obtaining high productivity.

INTRODUCTION

Currently there is worldwide interest in the development of catalytic processes for the production of chemicals from alkane feedstocks, replacing older technologies converting olefins (1). A recent example is the replacement of processes for benzene and butene conversion to maleic anhydride with modern technology using butane feedstock (2). For propane ammoxidation to acrylonitrile, it has been announced that BP America (formerly Sohio) is to commercialise a process in the near future (3). Such a process can be economically feasible compared with existing processes from propylene due to the difference in price between propane and propylene, which is currently of the order of 10 U.S. cents/lb (4). However, the propane ammoxidation process has to compete with the existing propylene processes, which give acrylonitrile selectivities of more than 80% at 98% of conversion per single pass (5). New propane ammoxidation technology also has to be competitive with a two-step process comprising a propane dehydrogenation unit together with conventional propylene ammoxidation technology. It has been reported that the latter two-step process would give 15–20% higher cost of production compared with a direct on-step propane ammoxidation process (6).

Different types of catalysts have been patented for propane ammoxidation, such as Bi–Mo–V scheelite-type (7) and rutile-type with Sb, V, W, Mo, and Al as key elements (8). Consideration of the data in the patents shows the latter catalyst system to be the most promising for industrial use. The Sb–V–(W, Mo)–Al–O system is very complex and in addition to the simple oxides it comprises phases such as $SbVO_4$, $AlVO_4$, and $AlSbO_4$. Possibly $AlSbO_4$ can form a solid solution with $SbVO_4$ (9). However, $SbVO_4$ is a crucial catalyst component (8) with two redox couples, Sb^{3+}/Sb^{5+} and $V^{3+}/V^{4+}/V^{5+}$, and it has been reported to have a cation-deficient rutile structure with the composition $Sb_{0.92}V_{0.92}O_4$ when prepared in air (10). If V_2O_5 and Sb_2O_3 are heated under an atmosphere strictly free of oxygen, a phase with the approximate composition $Sb_{0.95}V_{1.05}O_4$ is formed (11). Berry *et al.* have reported similar compositions (12). Mössbauer spectral data showed the antimony in both oxidised and reduced $SbVO_4$ to be present in the bulk exclusively in the pentavalent state (11), and consequently the vanadium is in the trivalent and tetravalent states.

Recent articles on propane ammoxidation over the rutile-type catalysts have been concerned mainly with the complex Sb–V–(Mo, W)–Al–O system (9, 13, 14). However, there is need for more detailed investigation of the Sb–V–O subsystem since such a study would create a

0021-9517/94 $6.00

better basis for understanding the more complex multicomponent catalyst system. The present study concerns the investigation of Sb–V–O catalysts for the ammoxidation of propane.

EXPERIMENTAL

Preparation of Catalysts and Reference Compounds

Catalysts with various Sb/V ratios were prepared by adding Sb_2O_3 (Merck, p.a.) to a warm solution of NH_4VO_3 (Merck, p.a.) in water, which was then heated under reflux with stirring for 16–18 h. The bulk of the water from the resulting slurry was evaporated on a hot plate under agitation until a thick paste had formed. The paste was then dried at 110°C for 16 h, and subsequently heated at 350°C for 5 h. After sieving the material, the fraction of particles in the range 150–425 μm was calcined at 610°C during 3 h in a flow of air. The catalyst notation and the corresponding Sb/V ratio and Sb/(Sb + V) fraction are given in Table 1 together with the specific surface area and the catalyst phase composition determined by XRD. For all samples the unit cell dimension of the $SbVO_4$ phase was found to agree with that reported for the oxidised form, i.e., $Sb_{0.92}V_{0.92}O_4$, which has a rutile structure with a = 0.4625 nm and c = 0.3040 nm (10).

For comparative purposes, two samples were prepared from V_2O_5 (Riedel-de-Haën, 99.5%) and Sb_2O_3 (Merck, p.a.) powders in the molar ratio 1 : 1, which were mixed by grinding and subsequently heated at 800°C for 2 h in air and in nitrogen free of oxygen, respectively. The former sample was the same as that previously used for crystal structure determination, according to which the product is pure, single-phase, and has a cation-deficient rutile structure with a composition close to $Sb(V)_{0.92}V(III)_{0.28}V(IV)_{0.64}\square_{0.16}O_4$, where □ denotes metal ion vacancies (10). The sample prepared in nitrogen gave an XRD pattern in agreement with data reported for the composition $Sb(V)_{0.95}V(III)_{0.95}V(IV)_{0.10}O_4$ (11), but weak lines from α-Sb_2O_4 were also noticed.

Characterisation of Catalysts

A Micromeritics Flowsorb 2300 instrument was used for the determination of specific surface areas, applying adsorption of N_2 at liquid N_2 temperature. Prior to measurement, the samples were degassed at 350°C for 3 h in nitrogen.

X-ray diffraction (XRD) analysis of the catalysts was carried out on a Philips X-ray diffraction instrument using a PW 1732/10 generator and Cu$K\alpha$ radiation.

Raman measurements were performed with a Bruker IFS66 FTIR spectrometer equipped with an FRA106 Raman device. A low power diode pumped Nd : YAG laser with an excitation line at 1046 nm and a liquid nitrogen cooled germanium diode detector were used. Measurements were carried out under ambient conditions on undivided catalyst particles in 5-mm NMR tubes. The power was usually set at 100 mW and the resolution was 8 cm^{-1}. Backscattering at 180° was measured and 4000 scans were averaged.

FTIR transmission spectra were collected on a Nicolet 20 SXC spectrometer equipped with a CsI beamsplitter, allowing recording down to 200 cm^{-1}. Disks containing 3 mg sample and 200 mg KBr were pressed. Spectra were recorded at room temperature in an atmosphere of dry air. The resolution was 2 cm^{-1} and 1000 scans were averaged.

X-ray photoelectron spectroscopy (XPS) measurements were performed with a Kratos XSAM 800 instrument using Mg$K\alpha$ X-ray radiation (1253.6 eV). The sample was attached to the sample holder with double-sided tape. Charging effects were overcome by mixing the sample with acetylene black (Carbon Philblack 1-ISAF from Nordisk Philblack AB). Spectra were recorded for the O 1s, Sb 3d, V 2p, C 1s, and Sb 4d spectral regions. The C 1s signal was set to a position of 284.3 eV. All catalyst samples were run twice, first without the addition of carbon black for determination of the Sb/V catalyst ratio and then with carbon black added for the measurement of band positions. For determination of atomic ratios the Sb $3d_{3/2}$ band was used for antimony, because the Sb $3d_{5/2}$ and the O 1s bands are very close and cannot be resolved. The V $2p_{3/2}$ band was used for vanadium since at high antimony content the intensity of the additional V $2p_{1/2}$ band is too low for quantification. Theoretical sensitivity factors for spectral analysis were recalculated and set as Sb 3d = 3.20 and V 2p = 1.30.

TABLE 1

Catalyst Notation, Composition, and Specific Surface Area

Catalyst notation	Sb/V	Sb/(Sb + V) (at.%)	BET area[a] (m^2/g)	Phase composition[b] (XRD)
Sb1V4	1 : 4	20.0	16.4	V_2O_5 + $SbVO_4$
Sb1V2	1 : 2	33.3	9.9	V_2O_5 + $SbVO_4$
Sb1V1	1 : 1	50.0	10.6	$SbVO_4$ + (V_2O_5 + α-Sb_2O_4)[c]
Sb2V1	2 : 1	66.7	3.6	$SbVO_4$ + α-Sb_2O_4
Sb3V1	3 : 1	75.0	4.3	$SbVO_4$ + α-Sb_2O_4
Sb4V1	4 : 1	80.0	2.6	$SbVO_4$ + α-Sb_2O_4
Sb5V1	5 : 1	83.3	1.4	$SbVO_4$ + α-Sb_2O_4
Sb6V1	6 : 1	85.7	2.5	$SbVO_4$ + α-Sb_2O_4
Sb7V1	7 : 1	87.5	1.3	$SbVO_4$ + α-Sb_2O_4

[a] The BET area for V_2O_5 and α-Sb_2O_4 used as catalysts was 7.8 and 0.6 m^2/g, respectively.

[b] The XRD data for $SbVO_4$ were in agreement with those reported in Ref. (10) for a rutile with the composition $Sb_{0.92}V_{0.92}O_4$.

[c] Traces.

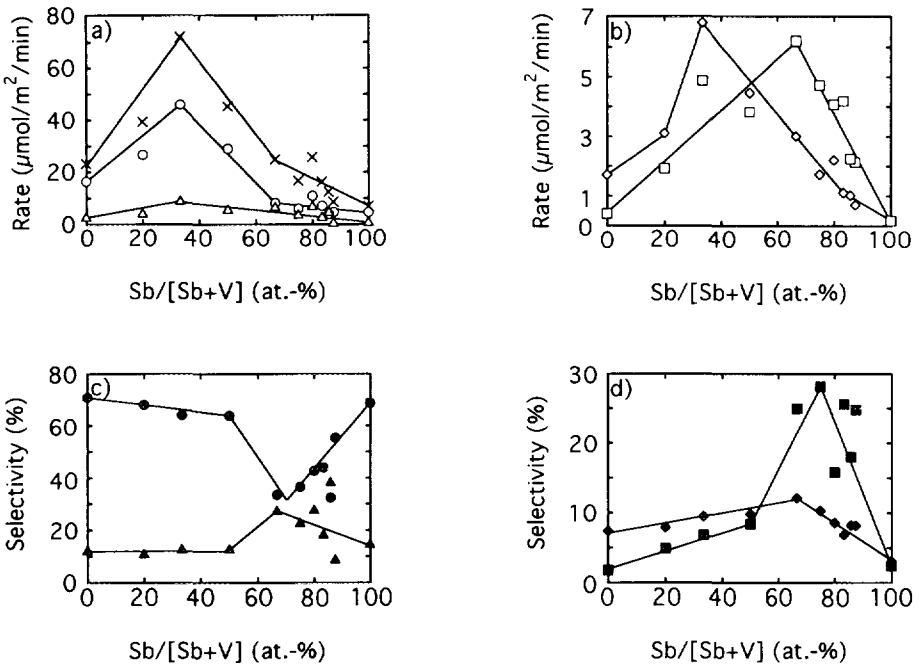

FIG. 1. Variation of rates and selectivities in propane ammoxidation with the fraction Sb/(Sb + V). (a) Rate for propane conversion (X) and rate for formation of propylene (○) and carbon oxides (△); (b) rate for formation of acrylonitrile (□) and acetonitrile (◇); (c) selectivity for formation of propylene (●) and carbon oxides (▲); and (d) selectivity for formation of acrylonitrile (■) and acetonitrile (◆). Experimental conditions: reaction temperature 480°C, mole ratio propane/oxygen/ammonia/water vapour/nitrogen = 2/4/2/1/5, and propane conversion 1–4%.

Temperature-programmed desorption of oxygen and subsequent reoxidation were carried out in pure argon and in argon with 1 vol.% of oxygen, respectively. The catalyst was placed in a quartz reactor which was heated in a furnace. A VG Pegasus mass spectrometer was connected to the outlet for analysis of oxygen.

A plug-flow reactor made of glass was used for the activity measurements. The catalyst sample was diluted with quartz grains to have isothermal conditions. Precautions were taken to avoid contribution from homogeneous reactions. In particular, dead volumes were reduced and hot zones were avoided in the tubing between the reactor and the analysis equipment. Nitrogen, oxygen, ammonia, propane, and water were dosed using mass flow regulators. The products were analysed on a Varian Vista 6000 gas chromatograph equipped with a Valco sample valve, an FID detector, a Porapak Q column, and a methaniser for the analysis of carbon oxides. Dependences on partial pressures of reactants and water vapour were studied sequentially by varying each pressure from low to high.

Catalyst samples were characterised before and after use in the catalytic reaction. For the latter purpose the samples were cooled to room temperature in the flow of reactants, but the flow of water vapour was stopped upon reaching 100°C.

RESULTS

Propane Ammoxidation over Sb–V–O Catalysts

In Fig. 1 reaction rates and selectivities for the formations of propylene, acrylonitrile, acetonitrile, and carbon oxides are given for low propane conversion as a function of the catalyst composition. In addition to these products, minor amounts of ethylene, methane, and HCN were formed. The total reaction rate is the highest for Sb1V2 (33.3 at.% Sb), and so are the rates for formation of propylene, carbon oxides, and acetonitrile. The rate for formation of acrylonitrile, on the other hand, is the highest for Sb2V1 (66.7 at.% Sb). Considering the selectivity data, Fig. 1 shows that the selectivity for propylene formation passes through a minimum and is the lowest for Sb2V1 (66.7 at.% Sb), while the selectivities for formations of carbon oxides, acrylonitrile, and acetonitrile all pass through maxima and are the highest for compositions rich in antimony. It should be noted, however, that the selectivity for propylene formation is high only at low propane conversion. With increase in conversion the selectivity for propylene formation over the vanadium-rich samples was found to decrease due to combustion. For the antimony-rich samples, on the other hand, the selectivity for acrylonitrile formation increases with increase in conversion due to the selective transformation of

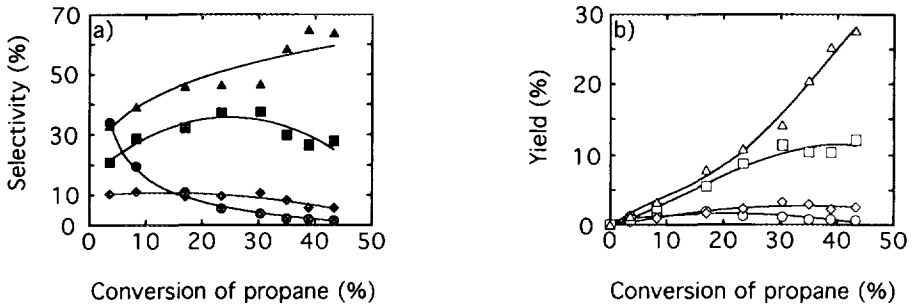

FIG. 2. Variation of selectivities and yields with propane conversion in propane ammoxidation over Sb2V1. (a) Selectivity for formation of propylene (●), acrylonitrile (■), acetonitrile (◆), and carbon oxides (▲); and (b) yield of propylene (○), acrylonitrile (□), acetonitrile (◇), and carbon oxides (△). Experimental conditions: reaction temperature 480°C, mole ratio propane/oxygen/ammonia/water vapour/nitrogen = 2/4/2/1/5, total flow 70 ml/min (STP), and weight of catalyst 0.2–5.0 g.

formed propylene (see Fig. 2a). Consequently, for the latter samples, when the selectivity for acrylonitrile formation is compared at higher conversion (≈30%) the maximum with catalyst composition becomes less pronounced. According to patents (8), the Sb/V ratio should be in the range 2–10.

The data in Fig. 1 point to the Sb2V1 sample as being the most interesting to explore further for acrylonitrile formation at higher conversion. Figure 2 gives yields and selectivities over this sample as a function of the propane conversion. For propylene formation the selectivity decreases with increase in conversion, while the selectivity for formation of carbon oxides shows the reverse behaviour. The selectivity for acrylonitrile formation passes through a maximum of about 37% at conversions in the range 20–30%. A selectivity around 10% is obtained for acetonitrile formation at low conversions, and it decreases with increase in conversion. The yields for formation of carbon oxides and acrylonitrile increase with increase in conversion. For acrylonitrile the highest yield, 11%, is obtained for a propane conversion of about 30–40%. The yields of propylene and acetonitrile are low and pass through maxima at 15 and 30% conversion, respectively.

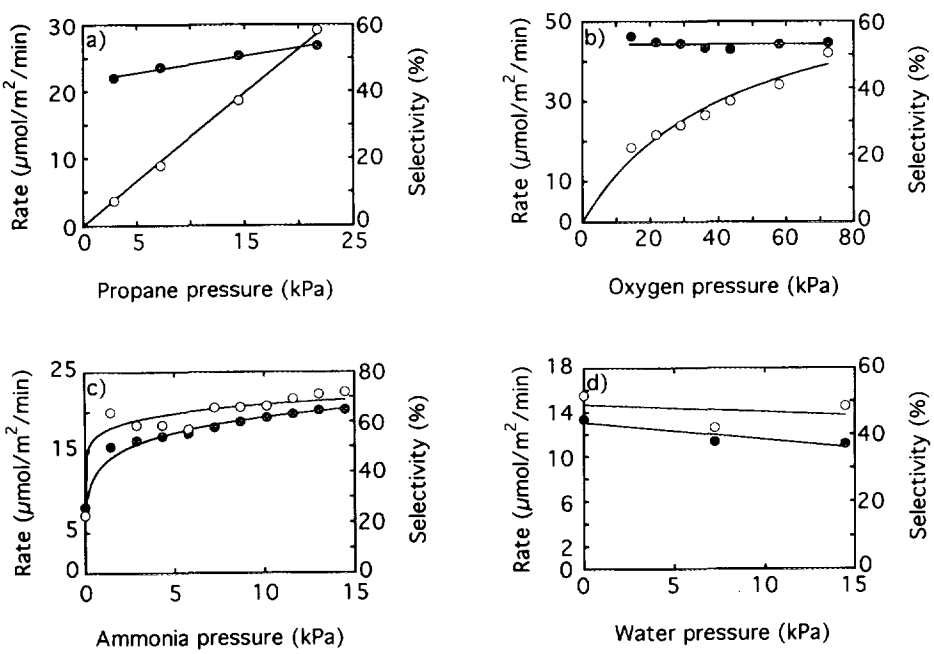

FIG. 3. Propane ammoxidation over Sb2V1. Rate (○) and selectivity (●) for propylene formation as a function of the partial pressure of (a) propane, (b) oxygen, (c) ammonia, and (d) water vapour. Experimental conditions: (a) oxygen 14.5 kPa, ammonia 7.2 kPa, and water vapour 7.2 kPa; (b) propane 14.5 kPa, ammonia 7.2 kPa, and water vapour 7.2 kPa; (c) propane 14.5 kPa, oxygen 14.5 kPa, and water vapour 7.2 kPa; and (d) propane 14.5 kPa, oxygen 14.5 kPa, and ammonia 7.2 kPa. Reaction temperature: 480°C. Data were obtained at differential conditions with conversions in the range 1–6%.

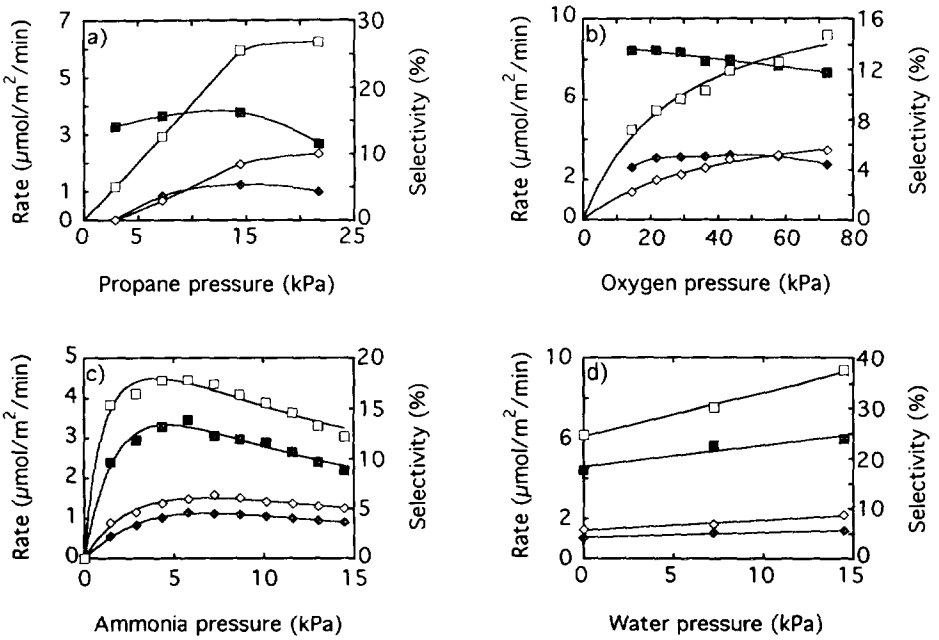

FIG. 4. Propane ammoxidation over Sb2V1. Rate (open symbols) and selectivity (closed symbols) for the formation of acrylonitrile (□, ■) and acetonitrile (◇, ◆) as a function of the partial pressure of (a) propane, (b) oxygen, (c) ammonia, and (d) water vapour. Experimental conditions are as in Fig. 3.

Influence on partial pressures of reactants. Figure 3 shows for Sb2V1 the rate and selectivity dependences on the partial pressures of propane, oxygen, ammonia, and water vapour for propylene formation. In Figs. 4 and 5 are the corresponding data for acrylonitrile and acetonitrile, and carbon oxide formation, respectively. The rate for formation of propylene shows a first order dependence on the partial pressure of propane, while the rates for formation of nitriles and carbon oxides follow a partial order dependence of Langmuir–Hinshelwood type.

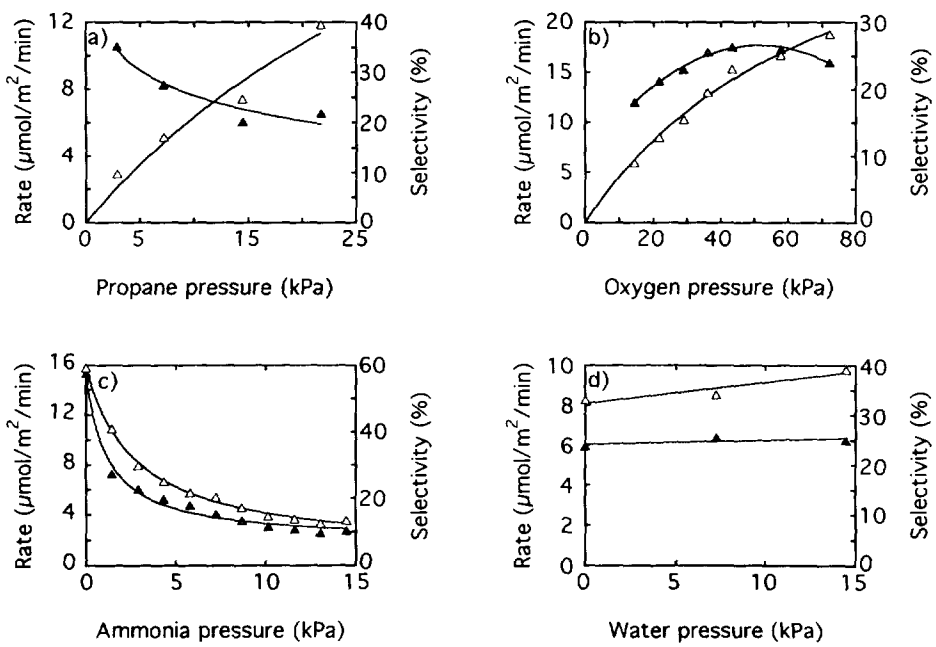

FIG. 5. Propane ammoxidation over Sb2V1. Rate (△) and selectivity (▲) for the formation of carbon oxides as a function of the partial pressure of (a) propane, (b) oxygen, (c) ammonia, and (d) water vapour. Experimental conditions are as in Fig. 3.

With increase in propane pressure the selectivity for formation of propylene increases, while the selectivity for carbon oxide formation decreases. The selectivities for formation of acrylonitrile and acetonitrile are almost independent of the partial pressure of propane and pass through weak maxima. When the partial pressure of oxygen is varied, the data in Figs. 3–5 show for all the products a Langmuir–Hinshelwood-type of rate dependence. The initial selectivities for the formations of propylene and nitriles show no strong dependence on the partial pressure of oxygen, whereas the selectivity for formation of carbon oxides increases with oxygen pressure and passes through a maximum. More complex dependences are observed with increase in the partial pressure of ammonia. At low ammonia pressure, the rate and the selectivity for formation of propylene increase rapidly and tend to almost constant values at high ammonia pressures. For acrylonitrile and acetonitrile formations, the rates and the selectivities pass through maxima as a function of the partial pressure of ammonia, while the rate and the selectivity for the formation of carbon oxides strongly decrease with increase in ammonia pressure. The dependences on the partial pressure of water vapour are weak and for acrylonitrile formation the selectivity and the rate of formation increase with the partial pressure of water vapour.

Characterisation of Catalysts

Catalyst samples were characterised by various techniques both as freshly prepared and after use in propane ammoxidation for 7 h under the conditions specified in the legend of Fig. 1. For comparisons, spectroscopic data for some reference compounds were also collected.

X-ray diffraction. XRD data for the used samples with Sb/V ratios above unity showed no significant differences compared with fresh samples, for which the phases present are given in Table 1. After use of the Sb1V1 sample in propane ammoxidation, the lines from crystalline V_2O_5 have disappeared, while the lines from $SbVO_4$ and α-Sb_2O_4 remain. Also, for Sb1V2, having an excess of vanadia compared with the stoichiometric amount needed for forming $SbVO_4$, the V_2O_5 lines disappeared upon use and no new lines from reduced vanadia appeared. The use of pure V_2O_5 in propane ammoxidation, on the contrary, gave a product which according to the XRD pattern predominantly consists of V_4O_9 (15), with a trace of V_6O_{13} (16).

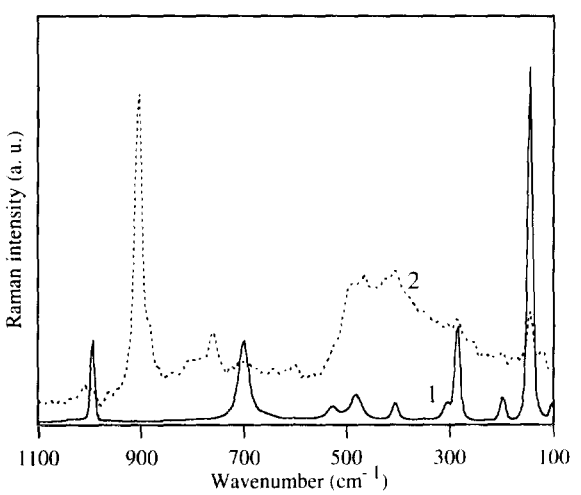

FIG. 6. Raman spectra of a catalyst freshly charged as V_2O_5. (1) fresh sample; (2) after use in propane ammoxidation.

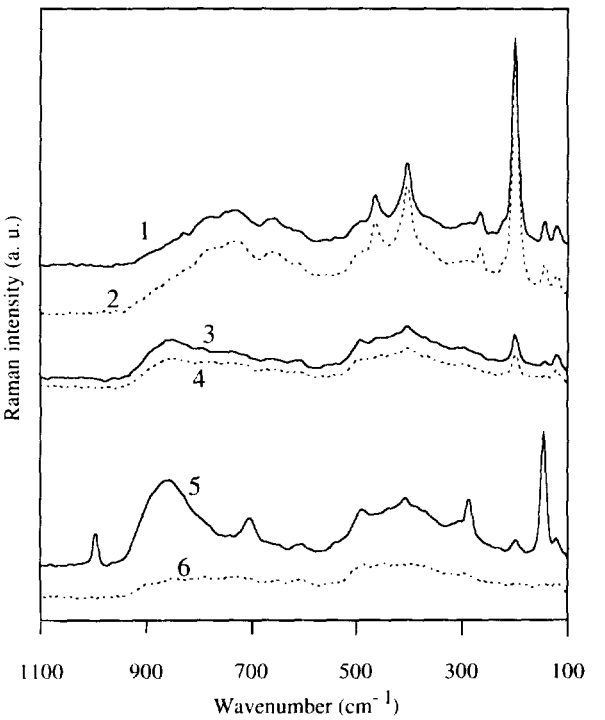

FIG. 7. Raman spectra of antimony–vanadium–oxide catalysts before and after use in propane ammoxidation. (1) Sb6V1, before use; (2) Sb6V1, after use; (3) Sb3V1, before use; (4) Sb3V1, after use; (5) Sb1V1, before use; and (6) Sb1V1, after use.

Raman Fourier transform spectroscopy. In Fig. 6 the spectrum of crystalline V_2O_5 is presented together with the spectrum recorded after its use in propane ammoxidation. The fresh sample shows bands that are typical for V_2O_5 (17); especially strong bands are at 145, 285, 700, and 995 cm^{-1}. After use the V_2O_5 bands have almost disappeared, and a new strong band appears at 906 cm^{-1} with a shoulder at 886 cm^{-1}. Less intense bands are at 407, 465, 762, and 1010 cm^{-1}. The presence of the new bands clearly shows that a reduction of V_2O_5 has occurred, and according to the XRD data V_4O_9 has formed.

Raman spectra for the Sb1V1, Sb3V1, and Sb6V1 samples are given in Fig. 7. These spectra representatively show the trends that were observed for the antimony vanadium oxide catalysts. All the strong bands for V_2O_5

(cf. Fig. 6) can be distinguished in the spectrum for freshly prepared Sb1V1. Additionally, there are some broad features in the ranges 800–930 and 350–520 cm^{-1}. After use in propane ammoxidation the V_2O_5 bands have disappeared and the two broad bands, especially that at 800–930 cm^{-1}, have markedly decreased in intensity. The spectra for Sb1V4 and Sb1V2 before and after use (not shown) showed features identical with those observed for Sb1V1 except for more intense V_2O_5 bands before use. After use the V_2O_5 bands had disappeared, and there were no bands from any reduced vanadia phase, not even in the spectrum for the used Sb1V4.

No bands from V_2O_5 are present in the spectrum for the fresh Sb3V1 sample, but below 500 cm^{-1} there are some spectral features from α-Sb_2O_4, of which the band at 200 cm^{-1} is the most intense (18). Additionally, the two broad features at 800–930 and 350–520 cm^{-1} are present, which were also in the spectra of the samples more rich in vanadium. After use of Sb3V1 in propane ammoxidation there is not much change in the spectrum; especially the α-Sb_2O_4 bands seem unaffected by the reaction. It is apparent that, comparatively, the broad band at 800–930 cm^{-1} has not decreased so much upon use as was the case for Sb1V1, Sb1V2, and Sb1V4. The Raman spectral features of the Sb2V1 sample before and after use were very similar to those shown here for Sb3V1.

For Sb6V1 there is almost no difference between the spectrum before and after use. All the sharp bands present are from α-Sb_2O_4 (18). A new broad feature appears at 600–800 cm^{-1}. This feature is very weak in the spectrum for Sb3V1, and it increases in intensity with increase in antimony content. Of the two other broad features that are typical for the antimony vandium oxide samples, the band at 800–930 cm^{-1} can be distinguished

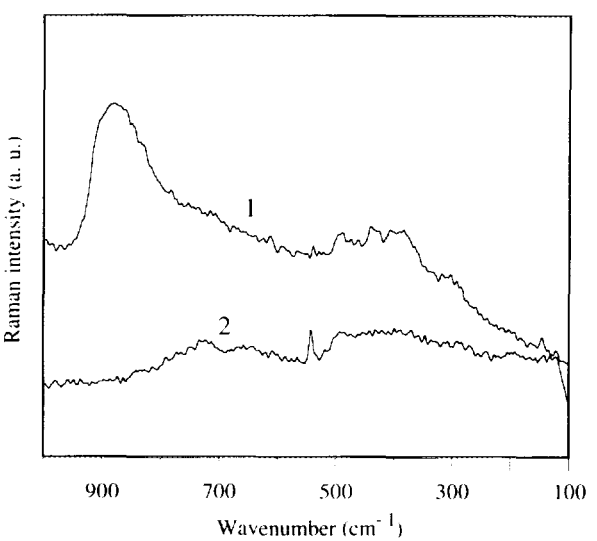

FIG. 8. Raman spectra of freshly prepared (1) $Sb_{0.92}V_{0.92}O_4$ and (2) $Sb_{0.95}V_{1.05}O_4$.

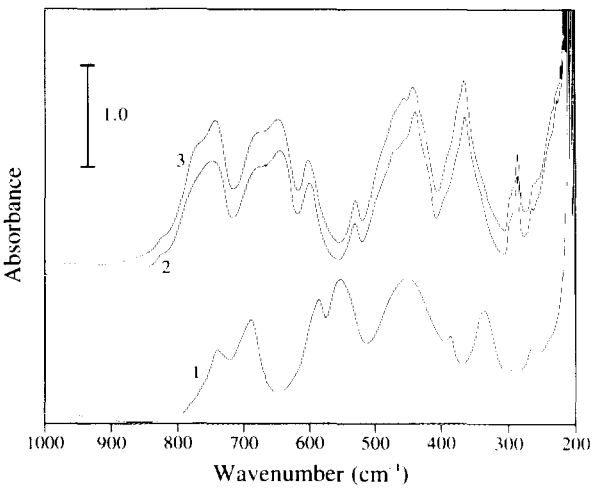

FIG. 9. Infrared spectra of some antimony oxides. (1) Sb_2O_3 (valentinite and senarmontite); (2) α-Sb_2O_4, freshly prepared; and (3) α-Sb_2O_4, after use in propane ammoxidation.

as a shoulder, and the band extending from 350 to 520 cm^{-1} is obscured by the bands from α-Sb_2O_4.

After use of a sample freshly charged as α-Sb_2O_4 in propane ammoxidation, the bands from α-Sb_2O_4 remained and there were no new bands showing reduction or phase transformation.

For comparison, the spectra of the reference compounds $Sb_{0.92}V_{0.92}O_4$ and $Sb_{0.95}V_{1.05}O_4$ are presented in Fig. 8. Both samples are quite bad Raman scatterers. The former sample has a band at 880 cm^{-1} and a less intense feature at 400–500 cm^{-1}, while the spectrum of the latter sample, except for an artefact peak at 542 cm^{-1}, shows only diffuse features. Comparison of the spectra in Fig. 7 for fresh antimony vanadium oxide catalysts with those in Fig. 8 shows that $Sb_{0.92}V_{0.92}O_4$ is a major catalyst constituent. The broad band at 600–800 cm^{-1}, which appears at very high antimony contents, is possibly from amorphous antimony oxide.

Infrared spectroscopy. Freshly prepared V_2O_5 gave a typical spectrum (17), and after use only features characteristic for V_4O_9 (15) were seen, with bands at 854, 885, 905, 928, 952, and 980 cm^{-1}.

Absorbance spectra of fresh and used α-Sb_2O_4 are shown in Fig. 9 together with the spectrum for Sb_2O_3 (Merck). The latter sample is a mixture of the valentinite and senarmontite phases, and the bands at 452, 555, and 585 cm^{-1} are from valentinite, while the band at 691 cm^{-1} is from senarmontite. Both phases have a band at 740 cm^{-1} (18). Comparison of the spectra for fresh and used α-Sb_2O_4 shows no reduction upon use forming new phases.

In Fig. 10 the infrared spectra of the oxidised and the reduced form of $SbVO_4$ are shown. The $Sb_{0.92}V_{0.92}O_4$

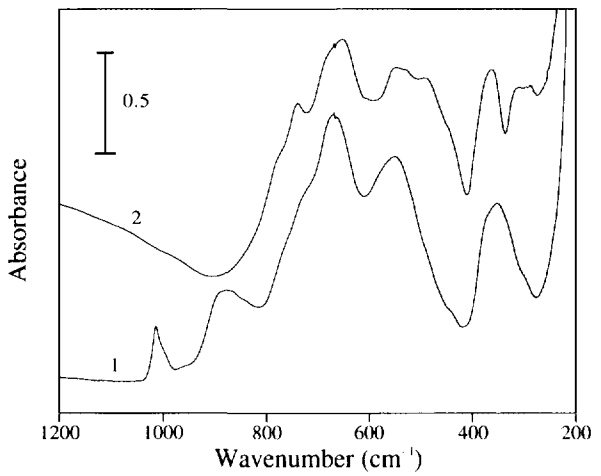

FIG. 10. Infrared spectra of $SbVO_4$ samples. (1) $Sb_{0.92}V_{0.92}O_4$; (2) $Sb_{0.95}V_{1.05}O_4$.

sample gives bands which are typical of the rutile structure (19, 20) at 362, 554, and 671 cm^{-1}, with a shoulder at 726 cm^{-1}. Bands at almost identical positions are present in the spectrum for $Sb_{0.95}V_{1.05}O_4$, but they are perturbed by some weak bands from α-Sb_2O_4 (cf. Fig. 9). Two more bands are present in the spectrum of $Sb_{0.92}V_{0.92}O_4$ at 880 cm^{-1} (broad) and 1016 cm^{-1}, positions that are close to those at 820 and 1020 cm^{-1} for two V_2O_5 vibration modes (17). However, the former bands are not from V_2O_5 contamination, a conclusion which is confirmed by the absence of V_2O_5 bands in the corresponding Raman spectrum (cf. Figs. 6 and 8) and the previous characterisation of this sample with electron microscopy, EDX analysis, X-ray, and neutron diffraction (10). Also, other investigators (11, 12) have found it possible to prepare a homogeneous sample in air, while preparations performed in the absence of gaseous oxygen always are contaminated with antimony oxide.

Some typical catalyst spectra are shown in Fig. 11, both before and after use in propane ammoxidation. The spectrum of the fresh Sb1V1 sample clearly shows some bands from V_2O_5 superimposed on the spectrum from the $Sb_{0.92}V_{0.92}O_4$ phase. V_2O_5 contributes to the absorbance around 1020, 830, and 400–600 cm^{-1}, and the band at 295 cm^{-1} is from V_2O_5 as well (17). After use of Sb1V1 in ammoxidation, the V_2O_5 bands have disappeared. The spectrum is now dominated by features from Sb–V–oxide and comparison with the spectra in Fig. 10 reveals the phase to be reduced, although incompletely so. For Sb2V1 there is no great change of the spectrum with use except for a general increase in intensity of bands, a feature that is common for all samples. The bands at 1016 and 880 cm^{-1} are from $Sb_{0.92}V_{0.92}O_4$, and there are several bands from α-Sb_2O_4 (cf. Fig. 9). Most bands in the two spectra for Sb7V1 are from α-Sb_2O_4, and almost no feature from Sb–V–oxide is apparent. The main difference in spectral features between the fresh and the used sample is the higher intensity of bands for the latter.

X-ray photoelectron spectroscopy. In Fig. 12 are shown the Sb $3d_{3/2}$ and V $2p_{3/2}$ binding energies plotted for the Sb–V–O catalysts before and after use in propane ammoxidation. Considering that the accuracy of XPS binding energy values generally is of the order ± 0.05 eV, it is clear the variation of the reported values is small. Despite this, however, some trends can be noticed. The Sb $3d_{3/2}$ binding energy value is identical for freshly prepared catalysts with Sb/V ≤ 1, while at higher ratios it decreases with increase in antimony content. Compared with fresh samples, after use in propane ammoxidation the Sb $3d_{3/2}$ binding energy is less for the samples with Sb/V ≤ 1 and higher for the samples that are richer in antimony. The binding energy value for vanadium is almost identical for the various fresh samples, except for Sb1V2 and Sb1V4, which have somewhat higher values. Upon use in propane ammoxidation the V $2p_{3/2}$ binding energy generally decreases by some 0.1–0.2 eV. The V $2p_{3/2}$ binding energy measured for V_2O_5 and pure $Sb_{0.92}V_{0.92}O_4$ was 517.1 and 516.8 eV, respectively, while that of Sb $3d_{3/2}$ for α-Sb_2O_4, Sb_2O_5 (Aldrich), and $Sb_{0.92}V_{0.92}O_4$ was 539.9, 540.3, and 540.2 eV, respectively.

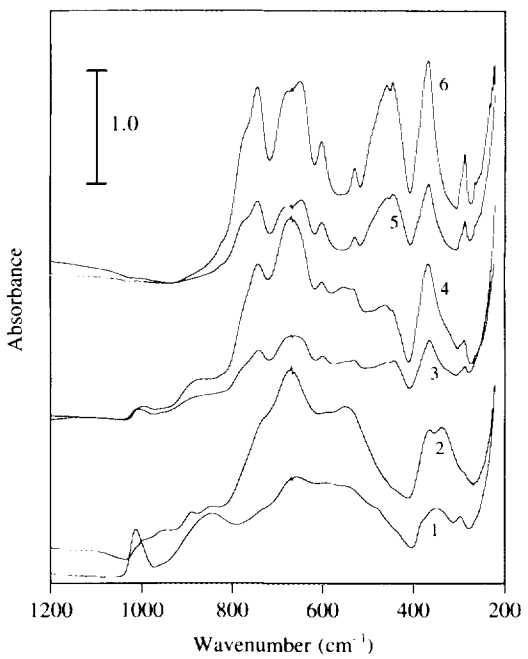

FIG. 11. Infrared spectra of some antimony–vanadium–oxide catalysts before and after use in propane ammoxidation. (1) Sb1V1, before use; (2) Sb1V1, after use; (3) Sb2V1, before use; (4) Sb2V1, after use; (5) Sb7V1, before use; and (6) Sb7V1, after use.

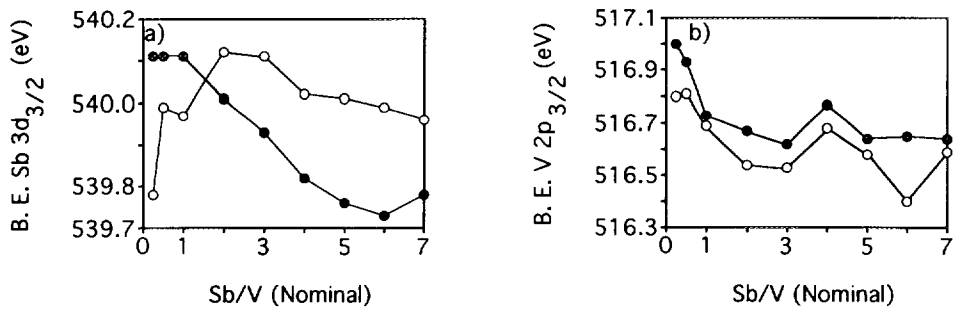

FIG. 12. XPS binding energies measured for the (a) Sb $3d_{3/2}$ and (b) V $2p_{3/2}$ peaks as a function of the nominal Sb/V ratio. Closed symbols, fresh samples; open symbols, after use in propane ammoxidation.

Considering the Sb/V ratios determined by XPS (Fig. 13), two different trends can be noted. In the vanadium-rich catalysts Sb1V4, Sb1V2, and Sb1V1, the Sb/V ratio decreases upon use in propane ammoxidation, whereas the reverse behaviour is observed for the samples with higher antimony content. The Sb/V ratio determined for the pure $Sb_{0.92}V_{0.92}O_4$ phase was 1.1 : 1.

Temperature-Programmed Desorption of Oxygen and Reoxidation

Temperature-programmed desorption of oxygen from the pure phase $Sb_{0.92}V_{0.92}O_4$, which according to the present results is a major catalyst constituent, was carried out in a flow of argon from ambient temperature up to 700°C. Figure 14 shows that desorption of oxygen starts at about 500°C, and that the rate of oxygen desorption reaches a maximum around 600°C. In subsequent treatment with 1 vol.% oxygen in argon, oxygen uptake occurs already at ambient temperature. During increase of temperature, the reoxidation rate attains a maximum at 560°C and the process is almost complete when reaching 700°C.

DISCUSSION

Structure of Antimony–Vanadium–Oxide Phases

Stoichiometric $SbVO_4$ cannot be prepared because the two redox pairs Sb^{3+}/Sb^{5+} and $V^{3+}/V^{4+}/V^{5+}$ make the oxidation/reduction process complex (21). Birchall and Sleight (11) reported the formation of $Sb_{0.92}V_{0.92}O_4$ when a mixture of Sb_2O_3 and V_2O_5 is heated in air at 800°C and the formation of $Sb_{0.95}V_{1.05}O_4$ together with Sb_2O_4 when the preparation is made in a sealed gold tube. Berry *et al.* (12, 21) made similar observations and reported the compositions $Sb_{1-y}V_{1-y}O_4$ and $Sb_{1-y}VO_{4-1.5y}$, $0 < y < 0.1$, for preparations made in air and oxygen-free nitrogen, respectively. Antimony Mössbauer data for the oxidised and reduced phases indicated that the antimony is predominantly in the pentavalent state (11). No evidence for an Sb^{3+} resonance was found, consequently indicating the bulk of the vanadium to be in the trivalent and tetravalent states. Recently, it was shown that $Sb_{0.92}V_{0.92}O_4$ has a cation-deficient rutile structure where the metal site contains a random mixture of 46% Sb, 46% V, and 8% vacancies (10). No evidence was obtained for an ordered distribution of cations, and considering that the metal site

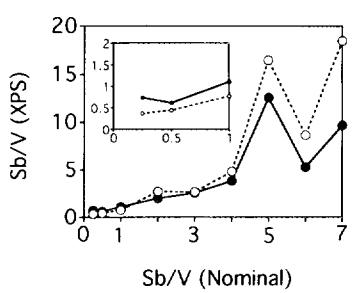

FIG. 13. The Sb/V ratio determined by XPS as a function of the nominal ratio. Filled symbols, fresh samples; open symbols, after use in propane ammoxidation.

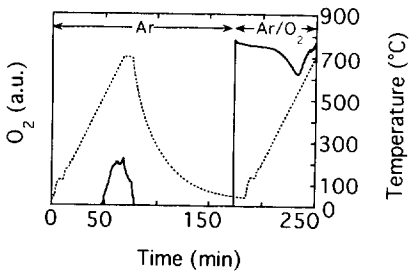

FIG. 14. Reduction and reoxidation of $Sb_{0.92}V_{0.92}O_4$. Temperature-programmed desorption of oxygen in argon, followed by subsequent reoxidation in an atmosphere with 1 vol.% of oxygen in argon. Solid line, oxygen signal; dotted line, temperature.

consists of six oxygens in a rather regular octahedron with two bond distances of 1.98 Å and four of 1.99 Å, the analysis showed preference for the Sb^{5+} and V^{3+}/V^{4+} bulk states. According to the XPS data in Fig. 12, however, the surface states are somewhat different from the bulk states. The binding energy (BE) value for Sb $3d_{3/2}$ in Sb1V1 (540.1 eV) and pure $Sb_{0.92}V_{0.92}O_4$ (540.2 eV) is intermediate between those for Sb_2O_4 (539.9 eV) and Sb_2O_5 (540.3 eV), indicating the presence of both Sb^{3+} and Sb^{5+} surface states. For vanadium the V $2p_{3/2}$ BE is 0.3–0.4 eV less than that for V_2O_5 (517.1 eV) and somewhat higher than reported for VO_2 (22), revealing a predominance for V^{5+} and V^{4+} surface states. Unlike a previous XPS study of $SbVO_4$ phases reporting an enrichment of antimony at the surfaces (23), the present data for Sb1V1 and the pure $Sb_{0.92}V_{0.92}O_4$ phase indicate the Sb/V surface ratio to be close to the bulk value. The discrepancy possibly is due to differences in synthesis conditions.

For the assignment of the Raman and infrared spectral features, it is worthwhile to note that in a stoichiometric rutile structure there is only one type of bulk oxygen species and all the cation positions are crystallographically identical (24). Each oxygen is bonded to three cations. In the cation-deficient oxidised phase $Sb_{0.92}V_{0.92}O_4$, in addition to 3-coordinated oxygens, as a consequence of the cation vacancies there are some 2-coordinated oxygens. It was shown that the 2-coordinated oxygens are in the following configurations given in sequence of probability Sb–O–Sb > Sb–O–V > V–O–V (10). The argument was that an oxygen bonded to two antimony atoms would require less distortion than is needed for the other two configurations as was shown by the formal valence for oxygen in an undistorted environment, which is −1.8, −1.4, and −1.1 for the Sb–O–Sb, Sb–O–V, and V–O–V configuration, respectively. The antimony-deficient reduced phase $Sb_{0.95}V_{1.05}O_4$ has a stoichiometric rutile structure without cation vacancies and thus all its oxygens are 3-coordinated. The infrared spectrum in Fig. 10 of $Sb_{0.95}V_{1.05}O_4$ in the region 200–800 cm^{-1} shows bands which, although perturbed due to bands from α-Sb_2O_4 contamination, are also evident in the spectrum of $Sb_{0.92}V_{0.92}O_4$. These bands are typical of rutiles and are from vibration modes involving the 3-coordinated oxygen (19, 20). Moreover, $Sb_{0.92}V_{0.92}O_4$ has two unique infrared bands at 880 and 1016 cm^{-1}, which thus possibly are from vibration modes involving the 2-coordinated oxygen species. Of these bands only the former is evident in the corresponding Raman spectrum in Fig. 8. The band at 880 cm^{-1} can be from a Sb–O–Sb stretching mode, since this configuration requires the least distortion of the octahedral structure unit. On the other hand, the band at 1016 cm^{-1} can be from the stretching mode of the second most favourable configuration Sb–O–V, and not from V_2O_5 contamination as was previously proposed (9). The oxygen in the Sb–O–V position may be located in a strongly distorted environment with one extremely short metal–oxygen bond, which is formed because of the more severe unsaturation this oxygen would have in a corresponding undistorted position.

Synergistic Effects in Ammoxidation over Sb–V–O Catalysts

The activity data in Fig. 1 reveal two synergy effects in propane ammoxidation over the Sb–V–O system. One effect concerns the $V_2O_5/SbVO_4$ region and appears as a maximum for Sb1V2 (33.3 at.% Sb) in total activity expressed per unit surface area. The XPS data in Fig. 13 for this region show that the Sb/V surface ratio decreases upon use, and is possibly caused by spreading under the influence of the catalytic cycle of vanadia over the $SbVO_4$ surface. Thus, the origin of the synergy effect can be explained either by the formation of a very active vanadia phase supported on $SbVO_4$ or by active grain boundaries between $SbVO_4$ and reduced amorphous vanadia. A reduction of vanadia is evidenced by the small decrease in the BE of the V $2p_{3/2}$ peak during propane ammoxidation (Fig. 12b), and the absence of XRD, Raman, and infrared bands from any reduced and crystalline vanadia confirms the formation of an amorphous structure.

The second synergy effect concerns the $SbVO_4/\alpha$-Sb_2O_4 region and is apparent in Fig. 1 as a maximum in the selectivity and the rate for acrylonitrile formation. The effect is related to the catalyst function for transformation of the intermediate propylene to acrylonitrile, as is evident considering the selectivity variations for propylene and acrylonitrile in Fig. 1. Other investigators have observed the same synergy effect in both propane ammoxidation (13) and propylene oxidation (25), and there is an agreement with data reported in the patents (8). However, the previous reports have only given results for few Sb/V ratios and have not emphasized exploring the origin of the synergy effect. According to the present results it is the migration of antimony over $SbVO_4$, modifying its surface, which most probably causes the synergy effect. Comparison of the Sb/V ratios determined by XPS between fresh and used catalysts having nominal Sb/V ratios greater than unity (cf. Fig. 13) shows that the surface ratio increases under the influence of the catalytic reaction. The observation that the BE of the Sb $3d_{3/2}$ peak for the same samples increases upon use (Fig. 12a) supports the view that migration of antimony occurs from the excess α-Sb_2O_4 with both Sb^{3+} and Sb^{5+} to the surface of $SbVO_4$, having higher preference for Sb^{5+} states. Migration of antimony from the bulk of $SbVO_4$ up to the surface does not occur because no increase in the Sb/V ratio upon use of pure $Sb_{0.92}V_{0.92}O_4$ was observed (26).

For the samples with a nominal ratio Sb/V $\leq$ 1, on the other hand, the BE of the Sb $3d_{3/2}$ peak decreases upon use due to reduction of the antimony in $SbVO_4$. The reduction agrees with the features of the Raman spectra for Sb1V1 in Fig. 7, showing that the broad band at 800–930 cm^{-1} has almost disappeared after use in propane ammoxidation. This band is from $Sb_{0.92}V_{0.92}O_4$ (see Fig. 8) and in the previous section was tentatively assigned to a Sb–O–Sb vibration mode. It has been established that Sb^{5+} is the element involved in oxygen and nitrogen insertion in propylene oxidation and ammoxidation, respectively, over $FeSbO_4/\alpha$-Sb_2O_4 and USb_3O_{10} (27). Therefore, the [Sb–O–Sb] sites of $SbVO_4$ are possibly active for the transformation of formed propylene to acrylonitrile in line with the observation that the intensity of the 800–930 cm^{-1} Raman band after use and the selectivity for acrylonitrile formation are both low for the samples with a nominal ratio Sb/V $\leq$ 1. The Raman spectrum of the used Sb1V1 sample in Fig. 7 resembles that of $Sb_{0.95}V_{1.05}O_4$ in Fig. 8, but the XRD data did not show complete reduction of $Sb_{0.92}V_{0.92}O_4$ in Sb1V1 to form $Sb_{0.95}V_{1.05}O_4$. Incomplete reduction is supported by the infrared spectrum in Fig. 11 for Sb1V1 after use in ammoxidation, which shows differences when compared with the spectra in Fig. 10 for $Sb_{0.92}V_{0.92}O_4$ and $Sb_{0.95}V_{1.05}O_4$. Especially the bands in the 800–1200 cm^{-1} region are more diffuse than is the case for $Sb_{0.92}V_{0.92}O_4$. Catalysts with nominal Sb/V ratios greater than unity, on the other hand, are selective for nitrile formation and do not show upon use a strong decrease in the intensity of the Raman and infrared bands at 800–930 cm^{-1} (see Figs. 7 and 11). The reason can be either faster reoxidation of [Sb–O–Sb] sites due to the new suprasurface sites created as a result of migration of antimony, or the suprasurface sites have taken over the function of the in-plane [Sb–O–Sb] sites. A more efficient reoxidation of the antimony sites is shown by the Sb $3d_{3/2}$ BE measured after use. It is worthy of note that the Sb $3d_{3/2}$ BE of the $SbVO_4$ surface in the catalysts with nominal ratios Sb/V > 1 is actually higher than the values in Fig. 12a suggest because these have a contribution from excess α-Sb_2O_4. The infrared spectra for Sb2V1 in Fig. 11 show that the band at 1016 cm^{-1} shifts toward a slightly lower wavenumber upon use. This can be due to reduction of some of the vanadium, in agreement with the change of V $2p_{3/2}$ BE depicted in Fig. 12b.

Ammoxidation Kinetics and Mechanism

The pressure dependences were studied at one temperature in series over the same catalyst sample, but the rates and selectivities show some minor changes with time on stream. Therefore the data collected are not primarily suited for the calculation of exact values for kinetic constants, but can well be used for a more general discussion of mechanistic features and influence of partial pressures and mole ratios of reactants.

Propane and $SbVO_4$ at about 500°C constitute a highly activated system. This is evident considering that propane is known to undergo oxidative dehydrogenation to propylene homogeneously above 500°C (28) and that the oxygen mobility in $SbVO_4$ is high, which is manifested by its loss of oxygen above 500°C (Fig. 14). Figure 3a shows for propylene formation a first order rate dependence on the partial pressure of propane, indicating that the adsorption of propane is the rate limiting step. Contrary to what has been proposed for propane ammoxidation over scheelite-type catalysts (29), the propylene is not formed homogeneously. This is proven by the dependences on oxygen and ammonia pressures shown in Figs. 3b and 3c, respectively, which are of the Langmuir–Hinshelwood type. A dependence of the partial pressure of ammonia on the rate for propylene formation has been observed in propane ammoxidation over a Sb–V–W–Al–O catalyst as well (30), and may be due to ammonia modification of the surface of $SbVO_4$ (31).

As opposed to propylene formation, the rates for formations of acrylonitrile, acetonitrile, and carbon oxides follow a partial order dependence on the propane pressure, cf. Figs. 4a and 5a. Such dependence implies that these products primarily are not formed directly from propane but from adsorbed propylene (see Fig. 2) in reaction pathways, each of which comprises a second slow step in addition to the preceding propane adsorption step. The true heterogeneous nature of these pathways is shown up by the dependences on oxygen in Figs. 4b and 5b, which are of the Langmuir–Hinshelwood type. Figure 4c shows that with increase in ammonia pressure the rates for the formations of acrylonitrile and acetonitrile pass through maxima, a behaviour that can be due to competitive adsorption between reactants (32), i.e., ammonia and formed propylene. For carbon oxide formation, Fig. 5c, the rate decreases with increase in ammonia pressure. Such a dependence was also observed for toluene ammoxidation and was explained as being due to competitive adsorption between ammonia and oxygen, resulting in a decrease of both the rate of reoxidation and the concentration of electrophilic oxygen species that are active for degradation (31, 33).

The discussion on the synergistic effect pointed to [Sb–O–Sb] sites as being active for the transformation of intermediate propylene to acrylonitrile. Concerning the first step in propane ammoxidation, i.e., the activation of propane to give propylene, an oxygen bonded to vanadium probably is active. This conclusion is supported by the fact that Sb1V1 and the other vanadium-rich samples are active and selective for propylene formation (cf. Fig. 1). In agreement with the solid state redox reaction be-

tween V_2O_5 and Sb_2O_3 forming $SbVO_4$ (10, 11), where the antimony is oxidised and the vanadium is reduced, it is most likely that a vanadium site is participating in the reoxidation of [Sb–O–Sb] and [Sb–NH–Sb] sites. This mechanistic view, supported by the present results, agrees with that expressed by Grasselli and co-workers in a general comment following a paper on propane ammoxidation (9).

Figure 2b shows a highest yield for acrylonitrile of 11% over Sb2V1 in agreement with results for the Sb–V–O system which are reported in the patents for similar reaction conditions and conversion levels (8), and according to which the key elements Al and W have to be added to obtain a substantially higher yield. Catani *et al.* (30) reported a yield of 35% for acrylonitrile formation in propane ammoxidation over a Sb–V–W–Al–oxide catalyst. The variations in Fig. 4 show that for obtaining a high rate and good selectivity for acrylonitrile formation it is advantageous to have propane, ammonia, and water vapour pressures of about 15, 3, and 15 kPa or higher, respectively. A high oxygen pressure increases the rate for acrylonitrile formation, whereas the selectivity decreases (Fig. 4b). Therefore, for oxygen a partial pressure of about 10 kPa seems to give a good balance, resulting in an optimum ratio for propane : oxygen : ammonia : water vapour equal to about 5 : 3 : 1 : 5. In the early patents a feed with higher concentrations of oxygen and ammonia compared to propane was used, while in more recent patents there has been a switch to a feed rich in propane, e.g., propane : oxygen : ammonia : water vapour = 5 : 2 : 1 : 1 (8). This ratio is for the reactants propane, oxygen, and ammonia close to that found best in the present work but the relative amount of water vapour is less. Considering that the data in Figs. 3–5 were obtained at differential conversion, evidently for industrial production less water has to be fed because the conversion is higher and the water vapour pressure increases along the reactor as water is produced in both selective and unselective reaction pathways. Also, a high water vapour content in the feed would decrease the productivity of acrylonitrile due the dilution effect. As a consequence of having a feed rich in propane, recycling of unconverted propane is required in industrial application and has been reported to be the case (3).

CONCLUSIONS

Kinetic measurements for propane ammoxidation over Sb–V–oxide catalysts reveal that a Sb/V ratio above unity is needed to have a catalyst formulation that is selective for acrylonitrile formation. The variations of selectivities and yields with the conversion of propane show that propylene is an intermediate in the reaction pathway from propane to acrylonitrile. Propylene formation follows a first order rate dependence on the partial pressure of propane and the dependences on oxygen and ammonia pressures are of the Langmuir–Hinshelwood type. These dependences show that the propylene is formed at the catalyst surface and that the adsorption of propane is rate limiting. For the formations of acrylonitrile and carbon oxides, the rate dependences on the partial pressure of propane are of partial order, indicating that these products are not formed directly from propane but from adsorbed propylene in pathways comprising a second slow step.

XRD patterns show that α-Sb_2O_4 and $SbVO_4$ (or more correctly $Sb_{0.92}V_{0.92}O_4$) are constituents in catalysts which are selective for the transformation of formed propylene into acrylonitrile. Correlation with XPS data shows this ability to be a consequence of the migration of antimony from α-Sb_2O_4 to the surface of $SbVO_4$ under the influence of the catalytic reaction, creating suprasurface antimony sites. A comparison of Raman and infrared spectra of vanadium-rich and antimony-rich catalysts before and after use in propane ammoxidation reveals the latter to be more efficiently reoxidised in the catalytic process. The infrared spectra for the oxidised and the reduced forms of $SbVO_4$, i.e., $Sb_{0.92}V_{0.92}O_4$ and $Sb_{0.95}V_{1.05}O_4$, respectively, show bands below 800 cm^{-1} that are typical of the rutile structure. However, the oxidised phase has two unique infrared bands 880 and 1016 cm^{-1}, of which the former is also apparent in Raman. Most probably these bands are from vibration modes involving the 2-coordinated oxygen, which is present in this phase due to the fact that 8% of the cation positions are vacant.

ACKNOWLEDGMENTS

Financial support from the Swedish National Research Council for Engineering Sciences (TFR) and the National Board for Industrial and Technical Development (NUTEK) is gratefully acknowledged.

REFERENCES

1. Wittcoff, H. A., *CHEMTECH* **20,** 48 (1990).
2. Malow, M., *in* "Handbook of Chemicals Production Processes" (R. A. Meyers, Ed.), Chp. 1.9. McGraw–Hill, New York, 1986.
3. Newsletter, *Appl. Catal.* **67,** N5 (1990).
4. Roth, J. F., *in* "Catalytic Science and Technology" (S. Yoshida, N. Takezawa, and T. Ono, Eds.), Vol. 1, p. 3. Kodansha, Tokyo, 1991.
5. Brazdil, J. F., *in* "Kirk–Othmer, Encyclopedia of Chemical Technology" (J. I. Kroschwitz, and M. Howe-Grant, Eds.), 4th ed., Vol. 1, p. 352. Wiley, New York, 1991.
6. Centi, G., Grasselli, R. K., and Trifirò, F., *Catal. Today* **13,** 661 (1992).
7. US Patents 4,760,154 (1988); 4,835,125 (1989); 4,837,191 (1989); 4,843,055 (1989).
8. US Patents 4,746,641 (1988); 4,784,979 (1988); 4,788,317 (1988); 4,871,706 (1989); 4,879,264 (1989).
9. Andersson, A., Andersson, S. L. T., Centi, G., Grasselli, R. K.,

Sanati, M., and Trifirò, F., *in* "Proceedings, 10th International Congress on Catalysis, Budapest, 1992" (L. Guczi, F. Solymosi, and P. Tetenyi, Eds.), Vol. A, p. 691, Akadémiai Kiadó, Budapest, 1993.
10. Hansen, S., Ståhl, K., Nilsson, R., and Andersson, A., *J. Solid State Chem.* **102,** 340 (1993).
11. Birchall, T., and Sleight, A. W., *Inorg. Chem.* **15,** 868 (1976).
12. Berry, F. J., Brett, M. E., and Patterson, W. R., *J. Chem. Soc., Dalton Trans.* 9, (1983).
13. Centi, G., Grasselli, R. K., Patane, E., and Trifirò, F., *in* "New Developments in Selective Oxidation" (G. Centi, and F. Trifirò, Eds.), Studies in Surface Science and Catalysis, Vol. 55, p. 515. Elsevier, Amsterdam, 1990.
14. Centi, G., Trifirò, F., and Grasselli, R. K., *Chim. Ind. (Milan)* **72,** 617 (1990).
15. Andersson, A., Bovin, J.-O., and Walter, P., *J. Catal.* **98,** 204 (1986).
16. Wilhelmi, K.-A., Waltersson, K., and Kihlborg, L., *Acta Chem. Scand.* **25,** 2675 (1971).
17. Abello, L., Husson, E., Repelin, Y., and Lucazeau, G., *Spectrochim. Acta. Part A* **39A,** 641 (1983).
18. Cody, C. A., DiCarlo, L., and Darlington, R. K., *Inorg. Chem.* **18,** 1572 (1979).
19. Rocchiccioli-Deltcheff, C., Dupuis, T., Franck, R., Harmelin, M., and Wadier, C., *C.R. Acad. Sci. Paris Ser. B* **270,** 541 (1970).
20. Husson, E., Repelin, Y., Brusset, H., and Cerez, A., *Spectrochim. Acta Part A* **35A,** 1177 (1979).
21. Berry, F. J., and Brett, M. E., *Inorg. Chim. Acta* **81,** 133 (1984).
22. Andersson, S. L. T., *J. Chem. Soc., Faraday Trans.* **75,** 1356 (1979).
23. Berry, F. J., Brett, M. E., Marbrow, R. A., and Patterson, W. R., *J. Chem. Soc., Dalton Trans.*, 985 (1984).
24. Andersson, A., *J. Solid State Chem.* **42,** 263 (1982).
25. Berry, F. J., and Brett, M. E., *J. Catal.* **88,** 232 (1984).
26. Nilsson, R., Lindblad, T., Andersson, A., Song, C., and Hansen, S., *in* "Preprints 2nd World Congress on New Developments in Selective Oxidation, Malaga, 1993."
27. Grasselli, R. K., Centi, G., and Trifirò, F., *Appl. Catal.* **57,** 149 (1990).
28. Burch, R., and Crabb, E. M., *Appl. Catal.* **A100,** 111 (1993).
29. Kim, Y. C., Ueda, W., and Moro-oka, Y., *Appl. Catal.* **70,** 189 (1991).
30. Catani, R., Centi, G., Trifirò, F., and Grasselli, R. K., *Ind. Eng. Chem. Res.* **31,** 107 (1992).
31. Andersson, A., Hansen, S., and Sanati, M., *in* "Structure–Activity and Selectivity Relationships in Heterogeneous Catalysis" (R. K. Grasselli, and A. W. Sleight, Eds.), Studies in Surface Science and Catalysis, Vol. 67, p. 43. Elsevier, Amsterdam, 1991.
32. Otamiri, J. C., and Andersson, A., *Catal. Today* **3,** 211 (1988).
33. Otamiri, J. C., and Andersson, A., *Catal. Today* **3,** 223 (1988).